Chemical Geology 712 (2026) 123427

Contents lists available at ScienceDirect

Chemical Geology

journal homepage: www.elsevier.com/locate/chemgeo

Research Paper

Radiogenic Sr isotopes reveal extended seasonal windows of soil-river dissolved organic carbon transfer in an Arctic permafrost catchment

P. Roux [a,*], C. Hirst [b], M. Villani [a], E. du Bois d'Aische [a], C. Osy [a], A.K. Kelley [c], J. Ledman [c], E.A.G. Schuur [c], S. Opfergelt [a]

[a] Earth and Life Institute, Université Catholique de Louvain, Louvain-la-Neuve, Belgium
[b] Department of Earth Sciences, Durham University, Durham, United Kingdom
[c] Center for Ecosystem Science and Society, Northern Arizona University, Flagstaff, AZ, USA

ARTICLE INFO

Editor: Oleg Pokrovsky

Keywords:
Permafrost
Dissolved organic carbon
Strontium isotopes
Arctic rivers
Talik
Soil-river connectivity
Shoulder seasons

ABSTRACT

Permafrost thaw mobilizes substantial quantities of dissolved organic carbon (DOC) to Arctic rivers. Yet the seasonal timing and sources of DOC transfer remain poorly constrained, particularly during shoulder seasons. In this study, we combine radiogenic strontium isotopes ($^{87}Sr/^{86}Sr$), water isotopes ($\delta^{18}O$ & δD), radiocarbon ($\Delta^{14}C$), and DOC, Sr and iron concentrations to investigate soil-river connectivity across contrasting seasons in Panguingue Creek, a headwater stream in Interior Alaska, USA.

Our dataset reveals that stream chemistry is primarily controlled by binary mixing between groundwater and a soil-derived source, with occasional inputs from snow/rainfall. Despite progressive seasonal soil thaw, the consistent stream $^{87}Sr/^{86}Sr$ signature indicates a singular source from soil organic layers. We quantify soil-derived contributions of 76% during Autumn, with detectable inputs persisting over 30 days beyond traditional summer monitoring periods. During Spring, soil-derived inputs are detected prior to ice break-up, contributing up to 35% as snowmelt mobilizes organic material across the watershed. Winter baseflow exhibits anomalous geochemical signatures (enriched $\delta^{18}O$, elevated $^{87}Sr/^{86}Sr$, ancient DOC with apparent ages of 5.0-7.2 ka), hypothesized to result from groundwater rerouting or year-round talik connectivity accessing isolated permafrost carbon.

These findings demonstrate that soil-river connectivity extends beyond conventional monitoring periods, implying that current Arctic carbon flux models may underestimate annual DOC export. As climate warming lengthens shoulder seasons, these previously unaccounted export windows will expand, increasing permafrost carbon release. Despite winter disconnection between rivers and active layers, talik could remain hydrologically connected, enabling continuous DOC mobilization throughout the year. Arctic headwaters require year-round monitoring as their direct connection to permafrost soils enables early detection of changes in soil-river transfer dynamics under rapid climate change.

1. Introduction

The permafrost region covers 21 million km^2 in the Northern Hemisphere (Obu, 2021) and contains approximately 1460-1600 Pg of organic carbon in near-surface (0–3 m) terrain, representing approximately one third of global soil carbon stocks and twice the stock of atmospheric carbon (Schuur et al., 2022). With Arctic temperatures rising at twice the global average (Bowen et al., 2020; Serreze and Barry, 2011), projections of permafrost thaw have estimated 14-69% of near-surface permafrost could thaw by 2100, (Meredith et al., 2019; Peng et al., 2023). Along with permafrost degradation, thawed organic matter could lead to critical climate feedback through the release of CO_2 and CH_4 that amplify surface warming (Burn et al., 2025; Schaefer et al., 2014; Schuur et al., 2015; Strauss et al., 2025; Turetsky et al., 2020), underscoring its potential impact on global climate (Jones et al., 2023).

Direct observations from a permafrost warming experiment indicate that 5-15% of soil organic carbon could be lost annually through hydrological pathways (Plaza et al., 2019; Rodenhizer et al., 2020). Arctic rivers serve as crucial conduits for transporting this mobilized carbon to the Arctic Ocean, with annual dissolved organic carbon (DOC) fluxes to

* Corresponding author.
E-mail address: philippe.roux@seismology.be (P. Roux).

https://doi.org/10.1016/j.chemgeo.2026.123427
Received 22 November 2025; Received in revised form 18 March 2026; Accepted 14 April 2026
Available online 15 April 2026

the ocean estimated at 25-36 Tg C yr^{-1} (Tank et al., 2023; Vonk et al., 2023, 2025). At the same time, riverine carbon transport could also lead to substantial release of CO_2 sourced from weathering processes (Humborg et al., 2010) and the breakdown of DOC in rivers via microbial and photo-oxidation (Bowen et al., 2020; Cory et al., 2014; Rocher-Ros et al., 2021). In-stream degradation of DOC is still poorly represented in current Earth System Models and could potentially offset terrestrial carbon uptake under accelerated warming (Mu et al., 2025). This emphasizes the critical need to understand and quantify carbon transfer between permafrost soils and rivers to accurately predict Arctic climate feedback (Koch and O'Donnell, 2025).

Climate change is also causing large hydrological changes in permafrost landscapes, which are altering the timing, amount and composition of carbon exported from soils to rivers (Neff et al., 2006; Shogren et al., 2020). These changes include earlier start of soil thaw, rising water tables, deepening active layers, and the formation of taliks, defined as zones of unfrozen soil that persist through winter (Devoie et al., 2024), whose prevalence is increasing under warming conditions (Farquharson et al., 2022; Jafarov et al., 2018; Parazoo et al., 2018). Altered precipitation patterns, with increasing rainfall replacing snow, further increase water table rise and enhance soil-river connectivity (Douglas et al., 2016; Kokelj et al., 2015). These hydrological shifts lead to an extension of the river export season, with earlier onset and longer duration of flow in Arctic headwater streams (Shogren et al., 2020). Shoulder seasons, defined as the spring ice break-up and autumn freeze-up periods, have emerged as critical, yet poorly constrained windows for carbon export (Beel et al., 2021; Finlay et al., 2006; Guo et al., 2012; Kelley et al., 2025a; Shogren et al., 2020; Townsend-Small et al., 2011). A meta-analysis of Arctic River data estimated that approximately 30% of annual DOC export from the Kuparuk River occurs during these shoulder periods (Shogren et al., 2020). However, most biogeochemical monitoring campaigns in permafrost catchments remain concentrated during open-water season, from June to August (Amon et al., 2012; Liu et al., 2022). Furthermore, the age and composition of exported DOC vary substantially across the hydrological year, with progressively older carbon exported as flowpaths deepen (Koch et al., 2022; Neff et al., 2006; Wild et al., 2019).

Permafrost thaw and changes in precipitation are also changing the source of DOC exported from soils to rivers. In this context, a long-term ^{14}C record of ecosystem and soil respiration indicates an overall aging of released carbon to the atmosphere, with occasional episodes of very low ^{14}C consistent with seasonal mobilization of old carbon controlled by soil temperature/thaw and moisture (Schuur et al., 2023). In conjunction, DOC, previously dominated by surface runoff during snowmelt and river ice break-up (Neff et al., 2006), may now also be increasingly derived from the following sources: (1) saturation of shallow soil layers yielding more degraded organic materials, (2) exposure of deeper soil horizons yielding older DOC from depth as the thaw season advances, (3) formation of taliks resulting in hydrological connectivity and a potential continuous export of DOC throughout the winter and beyond the traditional thaw season, and (4) thaw of older, previously frozen soil horizons resulting in occasional export of older DOC (Buckeridge and Grogan, 2010; Farquharson et al., 2022; Jafarov et al., 2018; Parazoo et al., 2018; Rushlow and Godsey, 2017; Schuur et al., 2023; Shogren et al., 2020; Tank et al., 2020; Treat et al., 2016). The DOC exported to rivers from these additional sources can result in a shift in the amount and timing of DOC that is degraded, stored or transferred along the land to ocean continuum (Catalán et al., 2021).

More than 99% of Arctic rivers drain small catchments (Vonk et al., 2023). As such, these small rivers provide direct signals of permafrost degradation that become diluted in larger systems (Shogren et al., 2019; Vonk et al., 2023). Small streams tend to show overall older DOC directly sourced from thawing permafrost (Dean et al., 2020; Mann et al., 2015; Schwab et al., 2020), whereas large Arctic rivers tend to be dominated by young, rapidly cycling organic matter containing bomb carbon from atmospheric nuclear weapons testing (Aiken et al., 2014; Neff et al., 2006; Raymond et al., 2007; Schwab et al., 2020; Spencer et al., 2015). Because of their direct connections to permafrost soils, first order streams provide direct signals of climate change impact that become masked in larger river systems, making them hotspots of hydrological and biogeochemical change (Finlay et al., 2006; Frey and McClelland, 2009; Vonk et al., 2019, 2023). However, it remains unclear how seasonal changes in permafrost soils and rivers shape the timing and sources of DOC transferred from soils to a headwater stream.

Radiogenic strontium isotopes ($^{87}Sr/^{86}Sr$) represent an ideal tracer for investigating soil-river carbon transfer processes in permafrost environments (Wortberg et al., 2017; Zhang et al., 2025). As no isotopic fractionation occurs during source-to-sink transfer, biological uptake or photochemical processes, Sr isotopes allow discrimination between the different sources (Bagard et al., 2013; Bataille et al., 2020; Capo et al., 1998; Chadwick et al., 1999; Mauclet et al., 2023; Monhonval et al., 2023; Reynolds et al., 2012). Arctic soil profiles can show large variations in $^{87}Sr/^{86}Sr$ ratios, with values consistently decreasing from organic-rich surface horizons into deeper mineral layers, reflecting the transition from weathered clay minerals in organic horizons to less radiogenic primary minerals in mineral horizons (Mauclet et al., 2023). This vertical gradient in $^{87}Sr/^{86}Sr$ ratios provides a powerful tool to track changes in soil contributions as hydrological connectivity and thaw depth evolve seasonally. Moreover, Sr isotopes have been shown to be effective tracers of iron oxide dissolution-precipitation in soils and rivers, making them well suited to trace the association between iron with DOC and fate during permafrost degradation and soil-to-river transfer (Hirst et al., 2022; Monhonval et al., 2023; Wortberg et al., 2017). Water isotopes ($\delta^{18}O$ and δD) complement $^{87}Sr/^{86}Sr$ ratios by tracing water masses (snow vs. rain) as well as groundwater dynamics, weathering processes, and evaporation effects, providing additional constraints on hydrological pathways (Birkle and Torres-Alvarado, 2010; Clayton et al., 1972; Gibson and Prowse, 2002; Karolytė et al., 2017; Matsuhisa et al., 1979; Putman et al., 2019). Finally, radiocarbon analysis ($\Delta^{14}C$) of DOC constrains its apparent age that in permafrost soil is related to depth of origin, yielding an integrated indicator of local thaw progression (Heaton et al., 2021; Schuur et al., 2008, 2015, 2023; Trumbore, 2000). Together, this multi-isotope approach enables quantitative assessment of the relative contributions from different soil depths and water sources to rivers across seasons.

To answer the question of how seasonal changes shape the timing and sources of DOC transfer from soils to a headwater stream, we combine DOC, Fe and Sr concentrations with Sr isotopes, water isotopes, and selected radiocarbon analysis on DOC, in a headwater stream from Interior Alaska, USA. We used stream water samples collected during contrasting periods of soil-stream connectivity: ice breakup during early shoulder season (Spring), open flow in early thawing season (Summer), ice freeze-up during late shoulder season (Autumn) and under-ice flow during the *Deep Cold* stage (Winter). This study utilizes typical mixing models to calculate contributions of different potential sources to stream chemistry. We hypothesize that: (1) Sr isotopes will track the contribution of DOC from different soil depths to stream DOC throughout the season, with deeper sources becoming increasingly important as thaw progresses; and (2) the transfer of DOC from soil to stream will extend beyond traditionally monitored thaw season, with shoulder seasons showing DOC contribution from chemically distinct sources.

2. Materials and methods

2.1. Study site

The study site for water collection is Panguingue Creek (PC) catchment, a second-order stream located in Interior Alaska, USA (63.87°N, 149.25°W), with a contribution area of approximately 66 km^2 (Fig. 1, U. S. Geological Survey, 2024). The catchment is situated at approximately 700 m elevation on a gentle, north-facing slope (~4°) in the northern foothills of the Alaska Range. The catchment lies within the

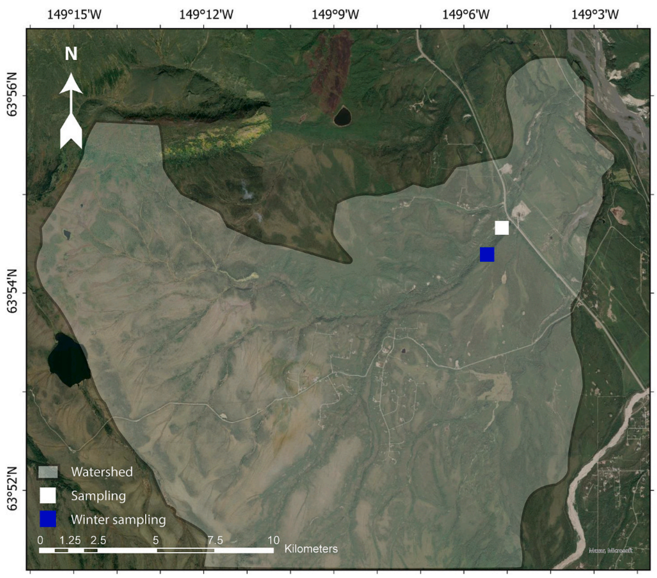

Fig. 1. Aerial photography of the Panguingue river catchment indicating the different sampling locations. Spring, Summer and Autumn are indicated as a white square while Winter is indicated as a blue square. Watershed boundaries are based on US Geological Survey data (U.S. Geological Survey, 2024).

discontinuous permafrost zones, and its underlying geology consists of Tertiary-aged sedimentary rocks, overlain by gravelly glacial till and wind-deposited silt, including the Pliocene Nenana Gravel. Surrounding soils are classified as Gelisols, with permafrost occurring within approximately one meter of the surface. Nearby soils are characterized by a surface organic mat (~0–10 cm) made up of moss and plant litter, underlain by organic-rich soil to about 40 cm depth, followed by mineral-rich soil layers composed of loess and glacial till (Osterkamp et al., 2009; Schuur et al., 2009).

2.2. Sampling

2.2.1. Definition of sampling periods

We separated soil-stream connectivity into two distinct hydrological pathways that vary seasonally, following the permafrost soil nomenclature established by Devoie et al. (2024). (i) Active layer-stream connectivity, when the seasonally thawed active layer is hydrologically connected to the PC stream; and (ii) Talik-stream connectivity, when hydrological inputs to the stream originate from taliks and permafrost through subsurface groundwater pathways, while the active layer remains seasonally frozen.

A total of 42 stream water samples were collected during four field campaigns between 2018 and 2024, representing distinct hydrological states of the PC stream and soil-stream connectivity.

Here we represented Autumn as the period including stream freeze-up, spanning September 6 - November 27, 2023 ($n = 19$). This period is characterized by the active layer of nearby soils at or near their seasonal maximum (Kelley et al., 2025b), resulting in peak soil-stream connectivity. It also includes both the onset of the refreezing process downward from the active layer surface causing shallow flow paths to progressively disconnect and stream discharge to recede (Supplementary Fig. S1).

Winter is represented as February 26 - March 6, 2024, ($n = 4$) and corresponds to the *Deep Cold* stage, characterized as a near-fully frozen stream channel, with under-ice base flow (Olsson et al., 2003). Surrounding soils have mostly frozen but contain taliks (Kennedy et al., 2025), resulting in no connectivity between active layer and stream, leaving taliks as the only potential subsurface connection (Devoie et al., 2024; Farquharson et al., 2022).

Spring is represented as the period including the river ice breakup spanning May 3-12, 2018 ($n = 9$). It is a brief, snowmelt-dominated period with little to no nearby soil thaw (Kennedy et al., 2025), causing a large rise in stream discharge and mobilization of organic material (Supplementary Fig. S1) while deeper horizons remain frozen and disconnected from the channel.

Summer is represented as the early thawing season, spanning June 8 - July 3, 2024 ($n = 10$). This period is characterized by an open stream near baseflow (Supplementary Fig. S1) and limited soil thaw (<30 cm; Kennedy et al., 2025), resulting in intermediate connectivity between active layer and stream, driven by the high hydraulic conductivity of soil surface organic layer (Schuur et al., 2009). It should be noted that this period best represents the first half of the summer thaw season that typically progresses through August into early September at this study site.

2.2.2. Environmental context of selected sampling periods

Air temperature for the different sampling periods showed typical seasonal patterns (Fig. 2a) with the highest air temperature during Summer (15.4 ± 2.7 °C, $n = 25$) and lowest during Winter (-20.0 ± 9.1 °C, n = 9) despite large spikes observed at that period (Fig. 2a). Spring and Autumn exhibit intermediary values with respective average air temperatures of 3.8 ± 3.5 °C (n = 10) and -0.3 ± 5.8 °C ($n = 52$). Overall, stream water temperature varied between -0.4 °C and + 13 °C and followed seasonal air temperature trend.

Because our sampling spans two hydrological years, we compared mean annual air temperatures for these sampling years against the decadal record (2014–2024) at the nearby Eight Mile Lake study site to assess whether interannual climate variability could influence our results (Supplementary Fig. S2; Supplementary Table S1). No sampling year differs significantly from the decadal mean (Wilcoxon test, $p >$ 0.05), indicating that our campaigns capture conditions representative of the broader climatic context.

Rainfall was limited throughout the combined 96 days of field campaigns, with no precipitation recorded for 59 of the sampling days (Fig. 2b). Of the 37 rainy days, 26 occurred during Autumn, 85% of which occurred before October. The remaining 11 rainy days were split between Summer (70%) and Spring (18%). The recorded rain in Winter resulted from the large increase in air temperature (Fig. 2a), leading to small amount of snowmelt. During Summer, 90% of rainfall events delivered less than 5 mm of precipitation, with only a single event exceeding this threshold.

Nearby soil temperatures also showed large seasonal variations (Kelley et al., 2025b). Winter had the coldest profiles, ranging from −9.5 to 1.5 °C over the first 40 cm, with a mean of −2.2 ± 1.8 °C and more than 95% of measurements below freezing. Spring averaged 0.0 ± 0.4 °C, with soil temperatures spanning only −1.7 to 3.5 °C and thaw depth remaining within the shallow organic layer at 6 ± 1 cm. Summer exhibited the warmest conditions, 3.8 ± 5.0 °C, more than 98% of measurements above 0 °C and a seasonal soil thaw depth of to 27 ± 16 cm. Deeper horizons (30–40 cm) remained partly frozen, with 35–49% of measurements still below 0 °C, indicating the presence of taliks at greater depth. During autumn, soil temperatures ranged from −8.2 to 15.6 °C, with a mean of 0.4 ± 1.5 °C, and thaw depth reached its seasonal maximum of 84 ± 25 cm by end of September. Autumn also showed progressive top-down refreezing, with the upper 20 cm fully refrozen by the end of November.

Field meteorological data and physical parameters indicate four distinct periods with contrasting soil–stream connectivity. This characterization allows us to test whether contrasting connectivity leads to contrasting DOC supply from soil to river.

2.2.3. Stream water sampling

Water sampling procedures were adapted to field conditions associated with each hydrological state. During Winter, stream waters were collected through a natural opening in the ice, located approximately 100 m upstream of the primary sampling site (63.90° N, 149.09° W;

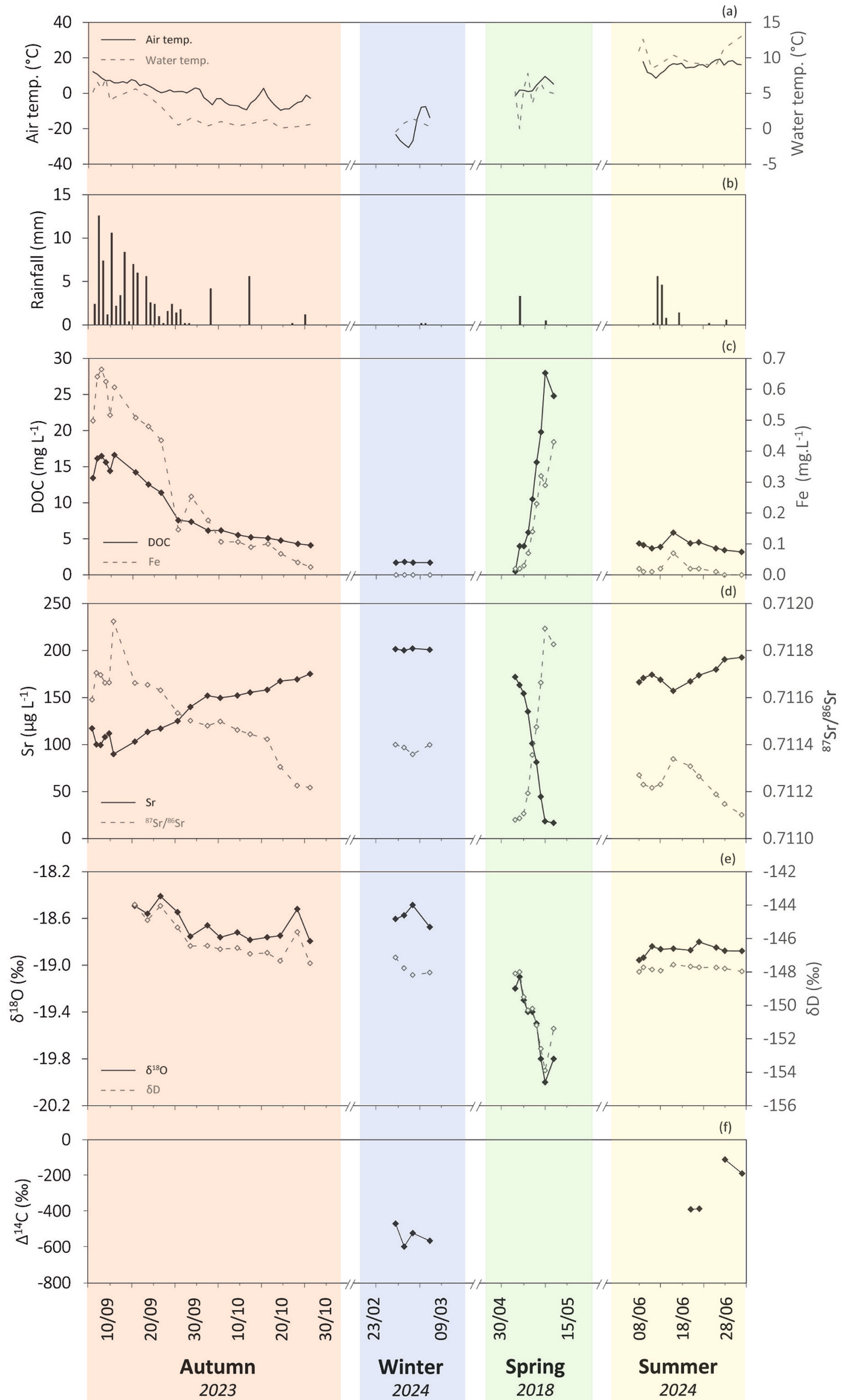

Fig. 2. Evolution of (a) air and stream water temperature, (b) rainfall, (c) DOC in mg L^{-1}, (d) Sr and $^{87}Sr/^{86}Sr$, (e) $\delta^{18}O$ and δD and (f) $\Delta^{14}C$ of stream waters collected in Panguingue Creek across all seasons.

Fig. 1), using a pre-cleaned polypropylene bottle. During Spring, prior to ice breakup in 2018, samples were obtained by drilling through the ice with an ice auger and retrieving water from beneath using a pre-cleaned plastic container attached to a non-metallic pole (Hirst et al., 2022). Following Spring ice breakup as well as throughout Summer and Autumn, stream waters were collected using a pre-cleaned 5 L polypropylene container or with the aid of a string, depending on stream discharge and accessibility.

2.2.4. Filtration and storage

Stream water samples were filtered within 10 h of collection. The samples intended for major element concentrations and Sr isotope analysis were filtered using a 0.2 μm nitrocellulose membrane filters (Millipore®). Samples intended for dissolved organic carbon (DOC) and radiocarbon analysis were filtered through 0.7 μm glass fiber filters (GF/F; Whatman®) that had been pre-combusted at 450 °C for four hours. All filtered samples were transferred to acid-washed polypropylene bottles and stored at 4 °C immediately following filtration or frozen for radiocarbon analysis. Samples intended for $\delta^{18}O$ & δD analyses were collected without filtration and stored in 20 mL polypropylene bottles that had not been pre-washed. The bottles were filled to minimize air presence and sealed with parafilm.

2.3. Analyses

All the data described in this section are reported in Supplementary Table S2. Data for the Spring samples are from Hirst et al. (2022), except for strontium parameters (Sr and $^{87}Sr/^{86}Sr$), which were measured in this study.

2.3.1. Colloidal fraction

To determine the proportion of elements transported as colloids and truly dissolved species within the filtered samples, a selection of water samples from Spring (n = 9) and Autumn (n = 12) periods underwent additional size separation. The colloidal fraction was defined as the 0.22 μm–1 kDa size fraction, while truly dissolved species were defined as the <1 kDa fraction. The colloidal proportion was calculated as the difference between truly dissolved and < 0.22 μm fractions. Size separation for Autumn samples was achieved using pressure filtration through 1 kDa filters (Ultracel® regenerated cellulose, 44.5 mm diameter). Unfiltered samples were placed in a pressurized container under 5 bars using N_2 gas. Size separation for Spring samples was performed using tubular dialysis membranes (Spectrapore 7®) following the protocol described in (Hirst et al., 2022).

2.3.2. Field parameters

Water temperature was measured in the field using a multi-parameter probe (Hanna Instruments). The measured field parameters for the Spring samples are available from Hirst et al. (2022). Rainfall data, air and soil temperatures as well as thaw depth were measured at the nearby Eight Mile Lake study site for all the sampling seasons (Kelley et al., 2025b; Kennedy et al., 2025).

2.3.3. DOC, Fe and Sr concentrations analyses

DOC concentrations in water samples from Autumn, Winter and Summer (n = 33) were determined using high-temperature catalytic oxidation (Shimadzu® TOC-VCPH). Fe concentrations were determined by ICP-OES Agilent 5800 VDV (Vertical Dual View). Sr concentrations were determined by inductively coupled plasma mass spectrometry (Thermo Fisher Scientific® iCAP Q ICP-MS). Detection limits for DOC, Fe and Sr are respectively 0.1 mg L^{-1}, 0.001 mg L^{-1} and 0.01 μg L^{-1} and accuracy are 5, 3 and 5%.

2.3.4. $\delta^{18}O$ and δD analyses

Analyses of water isotopes were performed on samples from Autumn, Winter and Summer using the Picarro L2130-i water isotope analyzer. Values are normalized using VSMOW2 and reported in per mil (‰) deviation relative to VSMOW. The reproducibility is evaluated on the USG47 standard reference material at 0.6‰ for δD and 0.1‰ for $\delta^{18}O$.

2.3.5. Radiocarbon analysis

A selection of eight water samples from Summer (n = 4; June 20th – July 2nd) and Winter (n = 4; February 27th – March 6th) were analyzed for radiocarbon signature at the Arizona Climate and Ecosystems (ACE) Isotope Laboratory (Northern Arizona University) following the method outlined in Lang et al. (2016). Briefly, to determine the radiocarbon signature of DOC, samples underwent wet chemical oxidation to convert them to CO_2, which was analyzed on a Miniaturized Carbon Dating System (MICADAS) with a carbonate handling system (CHS2) and gas interface system (GIS). DOC radiocarbon measurements were calibrated using gaseous OX-II and radiocarbon-dead CO_2 (IonPlus, Switzerland). A standard deviation of 8‰ and a blank radiocarbon age of 38,000 years are specified. Within our analyses, OX- II replicates had a standard deviation of 8‰. Samples were blank subtracted using the chemical glycine standard with an average radiocarbon age of 35,000 ± 2700 years (n = 32). Additionally, a replicate of a known environmental DOC sample was run on each day of analysis to assess instrument performance. Across 2 replicates representing the two days of analysis, the standard deviation of this internal standard was 3‰.

2.3.6. Radiogenic strontium analysis

The radiogenic strontium isotope analysis was performed on all water samples (n = 42) in a Class 100 clean laboratory under laminar flow conditions. Approximately 500 ng of Sr were evaporated on a hotplate at 90 °C. The resulting dry residue was digested using a mixture of H_2O_2 and HNO_3 (1:1) at 90 °C for 1 h, then evaporated to dryness. This oxidation step was repeated multiple times until no visible organic material remained. The residue was then re-dissolved in 100 μL of 3 M HNO_3. Strontium purification was performed using Biorad microspin columns loaded with 500 μL of pre-cleaned, Sr-selective resin (50–100 μm; Triskem), following protocol based on (Aciego et al., 2009). Procedural blanks accounted for less than 0.1% of the total Sr analyzed per sample.

Strontium isotope ratios were determined using a Multi-Collector Inductively Coupled Plasma Mass Spectrometer (MC-ICP-MS; Neptune Plus™) operating in wet plasma mode with a PFA nebulizer (100 μL min^{-1} uptake rate). Analyses were performed in a 2% HNO_3 matrix, with 8–10 V sensitivities achieved for 100 μg L^{-1} Sr. Each sample was measured in triplicate, and results are presented as the $^{87}Sr/^{86}Sr$ ratio. The reference material SRM987, used to validate column chemistry and analytical precision, yielded a $^{87}Sr/^{86}Sr$ ratio of 0.71027 ± 0.00002 (n = 27), consistent with the certified value of 0.71034 ± 0.00026.

At the PC catchment, exchangeable $^{87}Sr/^{86}Sr$ ratios in nearby permafrost soils were previously measured and showed a systematic decrease from 0.7122 in surface organic horizons (0–5 cm) to 0.7091 in the underlying mineral layers (30-50 cm) (Mauclet et al., 2023). This gradient provides us the ability to use $^{87}Sr/^{86}Sr$ ratios to detect changes in the soil horizon contributing to stream water across seasons. To do so, we used a standard three-endmember $^{87}Sr/^{86}Sr$ isotope mixing model to estimate the contribution of soil derived inputs, groundwater, and snowmelt to riverine Sr sources across seasons. The model assumes conservative mixing and defines endmember compositions based on observed 1/Sr and $^{87}Sr/^{86}Sr$ ratios trends:

$$f_{soil} \times [Sr]_{soil} \times \left(\frac{^{87}Sr}{^{86}Sr}\right)_{soil} + f_{gw} \times [Sr]_{gw} \times \left(\frac{^{87}Sr}{^{86}Sr}\right)_{gw} + f_{snow} \times [Sr]_{snow} \times \left(\frac{^{87}Sr}{^{86}Sr}\right)_{snow} = [Sr]_{stream} \times \left(\frac{^{87}Sr}{^{86}Sr}\right)_{stream}$$

where f_{soil}, f_{gw}, and f_{snow} are the contributions of soil-derived, groundwater, and snow/rain endmembers to stream Sr respectively; $[Sr]_{soil}$,

$[Sr]_{gw}$, and $[Sr]_{snow}$ are the Sr concentrations of each endmember; and $\left(\frac{^{87}Sr}{^{86}Sr}\right)_{soil}$, $\left(\frac{^{87}Sr}{^{86}Sr}\right)_{gw}$, and $\left(\frac{^{87}Sr}{^{86}Sr}\right)_{snow}$ are their respective isotopic compositions. The soil-derived endmember is based off exchangeable $^{87}Sr/^{86}Sr$ ratios measured by Mauclet et al. (2023).

3. Results and discussion

The evolution of air and stream water temperature, rainfall, DOC in mg L^{-1}, Sr and $^{87}Sr/^{86}Sr$ and $\delta^{18}O$ and δD and $\Delta^{14}C$ of stream waters collected in Panguingue Creek across all seasons are presented in Fig. 2.

3.1. Seasonal water isotopes variations

Water $\delta^{18}O$ ranged from −20.0 to −18.4‰ and δD from −153.9 to −144.0‰ across all seasons (Fig. 2e). The relationship between $\delta^{18}O$ and δD revealed distinct seasonal patterns relative to the Local Meteoric Water Line (LMWL; $\delta D = 7.8 \times \delta^{18}O + 2.9$; Fig. 3) primarily reflecting atmospheric processes (Putman et al., 2019). During low flow periods, isotope values remained relatively constant, with consistent values in Summer of −18.9 ± 0.07‰ for $\delta^{18}O$ and −147.8 ± 0.13‰ for δD, plotting close to the LMWL with a slight deviation below the line. This could reflect evaporation processes or groundwater inputs via water–rock interaction, but the limited summer variability does not allow us to discriminate between them (Birkle and Torres-Alvarado, 2010; Hirst et al., 2022; Karolytė et al., 2017; Putman et al., 2019). However, Winter exhibited an isotopic signature enriched in $\delta^{18}O$ values (−18.58 ± 0.08‰) compared to Summer, with similar δD (−147.8 ± 0.47‰), leading to a clear deviation from the LMWL indicative of enhanced water-rock interactions and/or additional groundwater inputs (Birkle and Torres-Alvarado, 2010; Karolytė et al., 2017). The shoulder seasons displayed the largest isotopic variations across seasons, both displaying a decreasing trend (Fig. 2e), but from different positions along the LMWL (Fig. 3). During Spring, both isotope systems showed a depletion trend from the Summer/Winter endmember toward the lower end of the LMWL ($R^2 = 0.93$). This decrease was characterized by $\delta^{18}O$ decreasing from −19.2 to −20.0‰ and δD from −148.1 to −153.9‰ which reflects an increasing influence of snowmelt (Gibson and Prowse, 2002; Hirst et al., 2022; Laudon et al., 2004; Streletskiy et al., 2015; Yi et al., 2010). Autumn showed a similar pattern, with samples plotting parallel to the LMWL but shifted toward higher $\delta^{18}O$ values. Isotopic compositions are progressively decreasing from enriched values in September (−18.49 ± 0.12‰ for $\delta^{18}O$ and −144.5 ± 1.2‰ for δD), close to previously measured soil perched waters under the influence of summer rain (Hirst et al., 2022; Putman et al., 2019), toward the Summer/Winter endmember by late autumn (−18.79‰ for $\delta^{18}O$ and −147.5‰ for δD; $R^2 = 0.88$). The parallel trend to the LMWL of Autumn samples likely reflects evaporation processes in soil water before transfer to the stream, although the relatively narrow isotopic range compared to previous studies on the same study site may mask a more distinct trend toward the LMWL (Hirst et al., 2022).

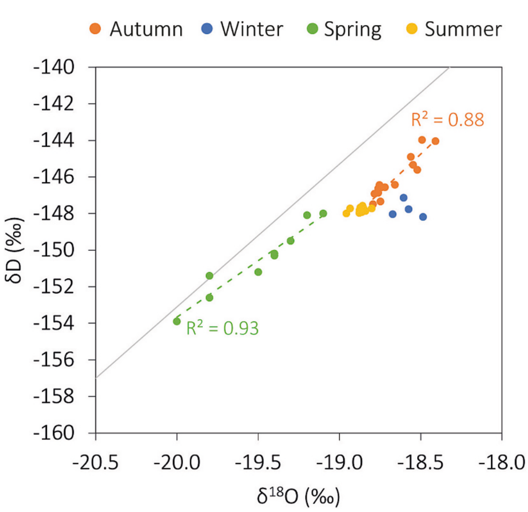

Fig. 3. Relationship between δD and $\delta^{18}O$ in stream water samples collected in Panguingue Creek across all seasons. The Local Meteoric Water Line (LMWL) is shown ($\delta D = 7.8\ \delta^{18}O + 2.9$).

3.2. Seasonal patterns, age, and inter-element relationships of DOC, Fe and Sr concentrations

3.2.1. Concentration patterns and seasonal variability

DOC concentrations spanned two orders of magnitude, ranging from 0.5 to 28 mg L^{-1}. During periods with little hydrologic variability and low rainfall inputs (i.e. Summer and Winter), DOC concentrations remained relatively constant, averaging 4.11 ± 0.75 mg L^{-1} during Summer and 1.73 ± 0.05 mg L^{-1} in Winter (Fig. 2c). In contrast, shoulder seasons exhibited large variations. During Spring, ice break-up led to a sharp increase in DOC concentrations from 0.50 to 28.0 mg L^{-1} within seven days, coinciding with snowmelt flush of organic material. Autumn data displayed the opposite trend, though at a much slower pace with DOC concentrations remaining stable in early September at 15.5 ± 1.3 mg L^{-1} (integrated over five days, $n = 5$) before gradually decreasing to 4.09 mg L^{-1} in late October.

Fe concentrations followed a similar pattern to DOC but over a narrower range, from 0.00 to 0.67 mg L^{-1} (Fig. 2c). Low river flow periods were characterized by minimal Fe concentrations, with no detectable Fe during Winter ($n = 4$) up to an average of 0.02 ± 0.02 mg L^{-1} during Summer. Spring was characterized by a sharp increase from 0.02 mg L^{-1} to 0.43 mg L^{-1} within nine days. During Autumn, Fe concentrations showed a progressive decrease from the highest Fe concentration recorded (0.67 mg L^{-1}) down to 0.03 mg L^{-1} over seven weeks. Together, these trends are consistent with a source likely derived from nearby soil active layers with Fe generated through redox cycling and mobilized with DOC before being exported to the stream.

Sr concentrations (Fig. 2d) exhibited the opposite pattern than DOC and Fe concentrations (Fig. 2c). They remained at a stable high level during Winter (201 ± 1 μg L^{-1}) and Summer (174 ± 11 μg L^{-1}), where the stream is close to baseflow. Values significantly dropped during ice break-up (Spring) with a 90% decrease within nine days to reach a minimum of 16.8 μg L^{-1} on May 12th, 2018. Conversely, Sr concentrations gradually increased during Autumn, ranging from 105 ± 10 μg L^{-1} in early September to 175 μg L^{-1} by late October 2023.

3.2.2. Radiocarbon signature and DOC age

Radiocarbon analysis of DOC revealed large seasonal differences in carbon age (Fig. 2f; Supplementary material Table S2). Summer samples exhibited a large range of $\Delta^{14}C$ values from −110‰ to −388‰, corresponding to apparent radiocarbon ages of 0.9 to 3.9 ka with an average of 2.5 ± 1.5 ka. In contrast, winter samples showed markedly more depleted (older) and a narrow range of values from −464‰ to −593‰, yielding apparent radiocarbon ages ranging from 5.0 to 7.2 ka with an average of 6.2 ± 1.0 ka. This represents the oldest DOC measured across our dataset, extending well beyond anything reported in arctic monitoring of stream dissolved load. Large Arctic rivers export predominantly modern DOC, with the oldest values observed in late Autumn, reaching −86‰ (Neff et al., 2006; Schwab et al., 2020). Similarly, headwater streams of Interior Alaska reported values up to approximately −200‰, with progressive aging as flowpaths deepened through the thaw season (Koch et al., 2022; O'Donnell et al., 2014). However, these ages are consistent with local soil carbon pool. At the nearby Eight Mile Lake study site, mineral soil layers to 85 cm depth contain organic matter with an age ranging from 2.5 to 4.5 ka BP (Lathrop et al., 2025), consistent with an increase in soil organic carbon age with depth (Schuur et al., 2023). Deeper profiles span from a maximum of 12.8 ka

BP at 1 m up to 40 ka BP at 5.5 m (Hutchings et al., 2019; Marshall et al., 2023). These values encompass our winter data while suggesting the winter source is most consistent with relatively shallow permafrost carbon rather than deep sub-permafrost groundwater. However, at such low winter DOC concentrations, even a small contribution of younger carbon would rapidly dilute older carbon signal (Barnes et al., 2018). The ~4 ka age offset between seasons indicates that winter baseflow accesses fundamentally different carbon pools than those mobilized during the active season. While summer DOC ages suggest a mixing of various carbon sources from the soil profile, the older winter values point to mobilization of carbon that has remained isolated from the active hydrological system for millennia (Schuur et al., 2023). Furthermore, the oldest summer values (3.9 ka) could suggest that this older component is a remnant of the winter source but becomes rapidly diluted or disconnected as discharge increases and shallower flowpaths dominate (Parazoo et al., 2018).

3.2.3. Inter-element relationships

The distinct seasonal trends observed for DOC, Fe and Sr concentrations result in characteristic inter-element relationships reflecting different mobilization and source processes. Together, Fe and DOC trends are consistent with a common, soil-derived source, mobilized together before being exported to the stream. The relationship between DOC and Fe concentrations reveals distinct seasonal patterns, with Spring samples characterized by higher DOC:Fe ratios than Autumn samples for similar Fe concentrations (Fig. 4a). Throughout the open river season, Fe is mainly transported as colloids (1 kDa - 0.22 μm; Hirst et al., 2022) where during Spring, Fe-bearing colloids are predominantly Fe-OC complexes sourced from the organic-rich litter and upper active layer and supplied to the stream through snowmelt-driven erosion (Hirst et al., 2022; Supplementary material Table S2). In contrast, during Autumn, a portion of the Fe-bearing colloids (with lower DOC/Fe ratio, Fig. 4a), are composed of iron oxides (e.g., ferrihydrite) (Hirst et al., 2022). These can form directly within the thawed active layer, where Fe (II) oxidizes through soil aeration prior to being transported to the river (Hirst et al., 2022). Alternatively, precipitation can occur during soil-to-river transport, at the redox interface of the riparian and hyporheic zones, where Fe(II)-rich subsurface waters meet oxygenated surface waters (Krickov et al., 2019, 2026).

The opposing seasonal trends in DOC and Sr concentrations reflect their contrasting sources, resulting in a strong inverse relationship across all seasons ($R^2 = 0.93$; Fig. 4b). Spring samples are characterized by high DOC and low Sr, consistent with snowmelt flushing of organic material (Hirst et al., 2022; Petrone et al., 2006). This signature progressively transitioned through Summer toward higher Sr and lower DOC, indicating increasing groundwater influence during baseflow conditions (Frey et al., 2007; Keller et al., 2010; Pokrovsky et al., 2015). Autumn samples showed intermediate concentrations but clustered closer to the DOC-rich end of the trend. This could be due to the samples being collected at the end of summer storm events where water is transferred through the surface organic-rich horizon, reactivating shallow soil layer DOC exports toward the stream (Fig. 2b) (Carey and Quinton, 2005; Koch et al., 2013). Later during Autumn, the data shifts toward the Sr-rich end of the trend, indicating an increasing groundwater influence as surface soil layers froze. Winter samples completed the pattern with high Sr and negligible DOC concentrations, consistent with groundwater influence under frozen conditions (O'Donnell et al., 2012).

3.3. $^{87}Sr/^{86}Sr$ ratios: sources and contribution calculations

3.3.1. Source identification and transfer mechanisms

The $^{87}Sr/^{86}Sr$ ratio in stream water samples ranged between 0.71108 and 0.71192 across all sampling campaigns, exhibiting seasonal patterns similar to those of DOC and Sr concentrations (Fig. 2d). Periods of low flow exhibit $^{87}Sr/^{86}Sr$ ratios that remained relatively constant, with an average of 0.71123 ± 0.00007 during Summer and 0.71139 ± 0.00002 during Winter. Winter values were consistently higher than other low flow periods (i.e. Summer and the end of Autumn), suggesting a contribution from more radiogenic sources during winter under ice. The shoulder seasons displayed contrasting patterns with $^{87}Sr/^{86}Sr$ ratios during Spring increasing rapidly from 0.71108 to 0.71189 alongside snowmelt and peak DOC concentrations. In contrast, Autumn showed $^{87}Sr/^{86}Sr$ ratios to start at elevated values in early September (0.71166 ± 0.00004, integrated over 5 days, $n = 5$) and gradually decreasing to less radiogenic values by late October (0.71122).

Analysis of the mixing diagram shows dissolved stream Sr to be controlled by three distinct endmembers (Fig. 5). Summer and Autumn samples align on a single straight mixing line, indicating two-endmember control. Considering the seasonal evolution of DOC, Fe, Sr, and $^{87}Sr/^{86}Sr$, these two endmembers are most consistent with groundwater and a soil-derived input. Spring samples deviate toward a third endmember consistent with rain/snowmelt due to the large dilution effect observed on Sr concentrations. Winter also deviates from the

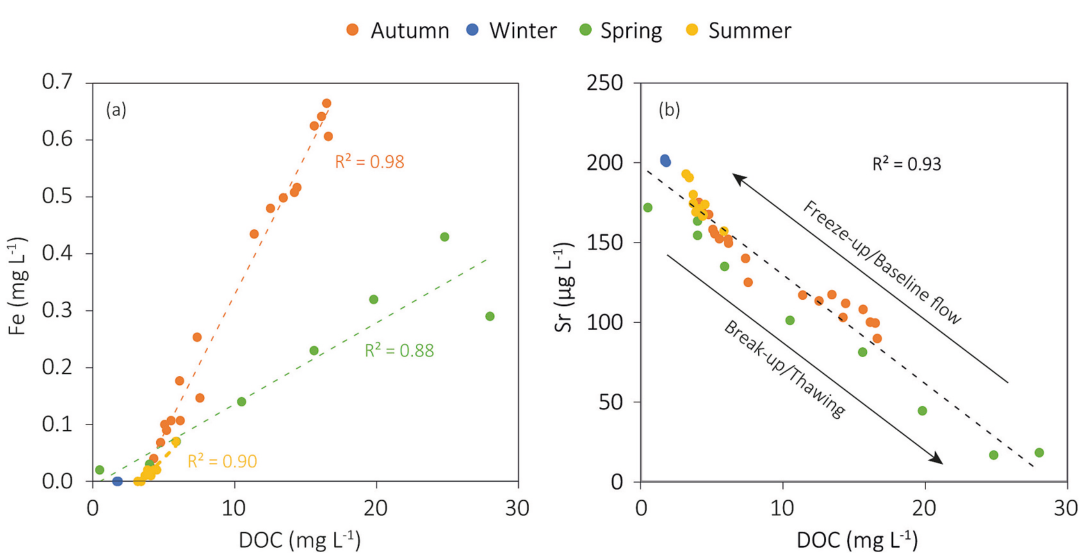

Fig. 4. Correlation between DOC (mg L^{-1}) and (a) Fe concentrations (mg L^{-1}) and (b) Sr concentrations (μg L^{-1}) in stream water samples collected in Panguingue Creek across all seasons.

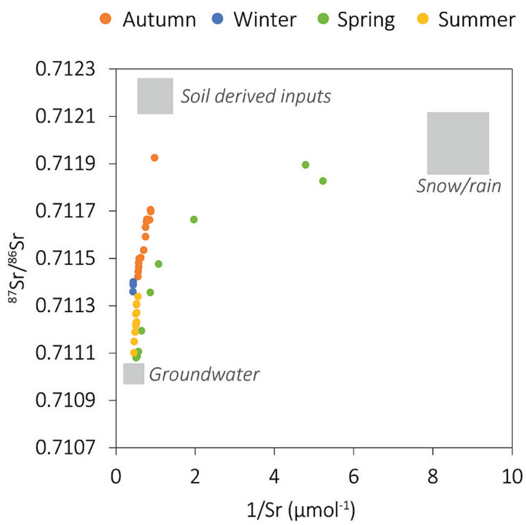

Fig. 5. Strontium isotope mixing diagram ($^{87}Sr/^{86}Sr$ vs 1/Sr) illustrating three-endmember mixing between soil-derived, groundwater, and snow/rain sources across seasons.

expected groundwater endmember despite no active layer-stream connectivity. The implications of this anomaly are explored in Section 3.5.

Our $^{87}Sr/^{86}Sr$ data reveal an unexpected pattern: the soil-derived $^{87}Sr/^{86}Sr$ ratio remains constant throughout all seasons, as evidenced by summer and autumn samples falling on the same mixing line. The absence of a progressive decrease of $^{87}Sr/^{86}Sr$ ratio throughout the season, which would have been expected if a deeper mineral horizons contributed increasingly to stream Sr as the active layer expanded to 84 cm by late autumn (Kelley et al., 2025b; Mauclet et al., 2023), confirms that stream Sr is dominated by a singular soil phase originating from the same integrated portion of the soil profile. This contradicts our initial hypothesis that progressive thaw would mobilize Sr from deeper soil horizons with distinct $^{87}Sr/^{86}Sr$ values (Mauclet et al., 2023). Together, the strong correlations between Fe, Sr and DOC and the narrow range of $^{87}Sr/^{86}Sr$ ratio suggest that soil-stream connectivity for Sr is likely the surface organic layer. This interpretation is supported by matching $^{87}Sr/^{86}Sr$ ratios between our soil-derived endmember and nearby topsoils (0.7122 $\pm$ 0.0001 for 0-5 cm, Mauclet et al., 2023), and by the high hydraulic conductivity of organic layers promoting lateral export to streams. Furthermore, we hypothesize this phase to be Fe-bearing colloids as they accumulate substantial quantities of Sr, with 20-40% of Sr reported to be bound to colloids in organic-rich soils (Hirst et al., 2022; Ilina et al., 2015; Monhonval et al., 2023; Pokrovsky and Schott, 2002; Stolpe et al., 2013). The consistent proportion of Fe transported as colloids (90–100% of Fe, Table S2) suggests that variations in DOC export are controlled by how much Fe is mobilized, with high erosive hydrological events (ice break-up, summer storms) increasing Fe colloid transport to rivers while during baseflow, reduced hydrological connectivity limits transfer to the river (Kelley et al., 2025a). In contrast, Sr shows to be transported via the colloidal fraction only during the earliest stages of Spring freshet, before shifting entirely to the truly dissolved fraction as the season progresses (Table S2). This behavior is consistent with previous observation in Arctic rivers where Sr tends to favor associations with organic ligands rather than organo-ferric phases (Krickov et al., 2019; Pokrovsky and Schott, 2002). Nevertheless, the strong inverse relationship between Sr and DOC concentrations likely reflects co-transfer through the same hydrological pathways and a shared source, despite different transport mechanisms than DOC and Fe.

In this context, it is necessary to note that unlike Sr, which behaves conservatively during riverine transport (Capo et al., 1998), DOC is subject to microbial degradation and photo-oxidation (Gagné et al., 2020; Mann et al., 2015; Rocher-Ros et al., 2021). In Arctic rivers, permafrost-derived DOC can be rapidly mineralized, particularly during baseflow when residence times are longer (Spencer et al., 2015; Wild et al., 2019). However, the strong correlation between DOC and Sr concentrations observed across all seasons in PC (Fig. 4b) suggests that DOC processing in-stream has not yet significantly decoupled DOC from its hydrological source, which could indicate short soil-to-river transfer time.

3.3.2. *Seasonal contribution calculations*

Using the different endmember sources of Sr defined in Section 3.3.1 we calculate the contribution of each source to the total dissolved stream Sr. The soil-derived inputs are characterized by a high $^{87}Sr/^{86}Sr$ ratio of 0.7122 $\pm$ 0.0001, constrained using average measured exchangeable $^{87}Sr/^{86}Sr$ data from nearby topsoil samples (0-5 cm depth, Mauclet et al., 2023), and a projected Sr concentration of 90 $\pm$ 10 µg L^{-1} derived from projected mixing trends. The groundwater endmember was characterized by projected mixing trends for both $^{87}Sr/^{86}Sr$ ratio and Sr concentrations, respectively set at 0.7110 $\pm$ 0.0001 and 250 $\pm$ 25 µg L^{-1}. The $^{87}Sr/^{86}Sr$ ratio of the groundwater endmember was set below the lowest measured datapoints as they still contain detectable Fe, suggesting contributions from soil-derived inputs. The lack of $^{87}Sr/^{86}Sr$ data on snow/rain lead to an endmember only constrained through projected mixing trends (0.7120 $\pm$ 0.0002) and measured Sr concentration (2.0 $\pm$ 1.5 µg L^{-1}, Hirst et al., 2022).

The resulting Sr contributions of the different endmembers are shown in Fig. 6. However, the Winter dataset deviates from the mixing model defined for the other seasons as it exhibits $^{87}Sr/^{86}Sr$ ratios that are inconsistent with the three identified endmembers with higher $^{87}Sr/^{86}Sr$ values than expected under river-ice. This deviation suggests additional processes or source modifications unique to winter conditions and are therefore excluded from contribution calculations. The implications of this anomaly are explored in Section 3.6. Across Spring, Summer and Autumn, groundwater appears to be a consistent contributor to stream Sr with an average contribution of 37 $\pm$ 19%. Soil-derived contributions dominate in Autumn, with an average Sr contribution of 61%, transitioning from 76% in early September to 35% in November. During Spring, this contribution evolves from 12% to 35% in the span of a week as snowmelt mobilizes organic material across the watershed, while snowmelt rapidly becomes the dominant source, reaching a maximum of 87% by May 12. During Summer, groundwater contributions dominate with an average of 57 $\pm$ 7% while soil-derived contributions average 36 $\pm$ 9%, peaking at 49% in mid-June before declining toward baseflow conditions.

3.4. *Prolonged soil-river connectivity during shoulder seasons*

Our $^{87}Sr/^{86}Sr$ strongly supports our second hypothesis that soil influence on stream chemistry extends well beyond traditional monitoring periods (Shogren et al., 2020). While previous work has estimated that traditional ice break-up sampling underestimates DOC export by ~30% (Finlay et al., 2006; Guo et al., 2012; Shogren et al., 2020; Townsend-Small et al., 2011), our data suggest this underestimation may be even more substantial. In this context, a recent study on the same study site estimated Spring freshet to be accounting for 59% of yearly DOC flux alone (Kelley et al., 2025a), consistent with spring freshet contributions of 40–60% of annual DOC export documented in larger permafrost-influenced Arctic rivers including the Pechora and Severnaya Dvina (Chupakov et al., 2020, 2023). However, these large river datasets do not capture the late shoulder-season tail-off in soil connectivity that we document here, suggesting that the full magnitude of annual DOC export remains systematically underestimated even in well-monitored Arctic river systems.

During Spring in the PC river, we detected soil-derived inputs in PC waters several days before complete ice break-up (May 7-9), with contributions to stream Sr reaching 35% (Fig. 6) which has also observed in large Arctic rivers (Juhls et al., 2020; Opfergelt et al., 2024). This likely

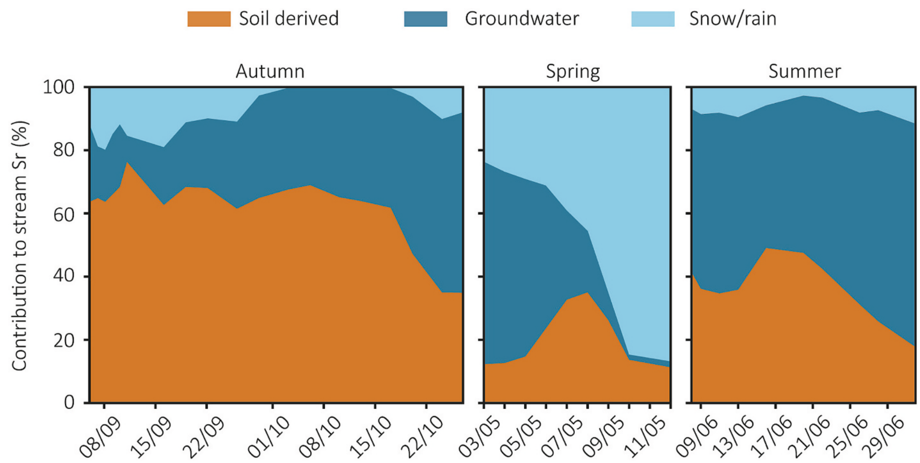

Fig. 6. Seasonal contributions of groundwater, soil-derived, and snow/rain inputs to Panguingue Creek stream Sr, calculated using a mixing model based on $^{87}Sr/^{86}Sr$ ratios. Winter samples are excluded as their $^{87}Sr/^{86}Sr$ values fall outside the three-endmember mixing framework defined for the other seasons (see Section 3.6).

results from snowmelt mobilizing DOC across the PC watershed before complete ice break-up, which occurs at different rates and timings spatially. While this early season extension is relatively brief (days), it captures the initiation of the spring DOC pulse.

During Autumn, our data demonstrate that soil-river connectivity persists well beyond traditional cutoffs. Previous studies typically define the end of the export season as plant senescence (September in our region), yet we observed sustained soil contributions throughout Autumn. From 64% in early September, coinciding with maximum active layer thickness at our site (84 ± 25 cm; Kelley et al., 2025b), declining to 35% by late October during the onset of top-down refreezing (Kennedy et al., 2025), thus representing over a month of additional export not captured in standard monitoring (Fig. 6). This extended soil-stream connectivity likely continues into the early winter phases (*Early Snow* and *Early Cold*; Olsson et al., 2003), before complete active layer disconnection during *Deep Cold*, as evidenced by undetectable Fe and minimal DOC in our Winter samples (Fig. 2c & 4a).

3.5. The curious case of winter

Under stream ice, the system appears to disconnect from the established soil-derived inputs-groundwater-rainfall system that characterizes other seasons (Fig. 5). This deviation is first evident in the $^{87}Sr/^{86}Sr$ data, which show elevated ratios that exceed values predicted by the three-endmember mixing model, indicating inputs that fall outside the established source mixing trends (Fig. 5). Furthermore, undetectable Fe concentrations and minimal DOC concentrations reinforce this interpretation by ruling out active layer contributions (Figs. 2 & 4). Water isotope data suggest an influence of water-rock interactions (Fig. 3) with Winter samples exhibiting enriched $\delta^{18}O$ values while maintaining similar δD compositions compared to Summer creating a clear departure from the LMWL (Clark and Fritz, 1997; Clayton et al., 1972; Karolytė et al., 2017; Matsuhisa et al., 1979). The radiocarbon data of DOC provides additional constraints on this winter source. The markedly older DOC age in winter compared to summer (Table S2) indicates access to an ancient carbon pool not detected during other seasons. This old DOC suggests groundwater flow in contact with old permafrost carbon. Notably, the Sr-DOC relationship being preserved through Winter indicates that this deeper flowpath is likely in contact with the same mineralogy as other seasonal pathways.

Our hypothesis is that winter conditions cause a rerouting of groundwater flow due to ice formation in subsurface pathways (Alsafi et al., 2024; Carey and Woo, 2002). As permafrost dynamics evolve seasonally, unfrozen pathways above, within, and below permafrost can allow interaction between groundwater and surface water (McKenzie and Voss, 2013; Walvoord et al., 2019). During the growing season, supra-permafrost flowpaths dominate DOC delivery, but under fully frozen conditions, deeper sub-permafrost or talik-connected flow may become the primary pathway to the stream (Vonk et al., 2019; Walvoord and Striegl, 2021). Alternatively, though less likely, ice may simply block major groundwater inputs to the PC stream (Alsafi et al., 2024), artificially increasing the influence of a single channel with an enriched $\delta^{18}O$ signature, more radiogenic Sr and in contact with older permafrost, but similar overall chemical profile, which is plausible given the numerous channels observed across the PC watershed (Fig. 1). It is also possible that this winter source represents talik-stream connectivity, persisting at low levels throughout the year but remaining largely masked by dominant inputs of younger DOC from soil organic horizons during the active season (Koch et al., 2022; Parazoo et al., 2018; Vonk et al., 2019; Walter Anthony et al., 2024), as suggested by summer $\Delta^{14}C$ values (Supplementary Table S2), despite shift observed in $^{87}Sr/^{86}Sr$ data (Figs. 2 & 5).

4. Conclusion and implication under future climate

Our study aimed at characterizing how seasonal changes in permafrost soils and streams shape the timing and sources of DOC transferred from soils to the Panguingue stream.

Our findings revealed that PC stream chemistry is primarily controlled by binary mixing between groundwater and a singular soil-derived source, with occasional rainfall/snowmelt inputs during hydrological transitions (e.g., river ice break-up). We quantified soil-derived Sr contributions reaching up to 35% during Spring and 76% during Autumn. These contributions were detected prior to ice break-up (12-35% Sr contribution) and persisted for over 30 days after typical late-season monitoring (35% Sr contribution in late October).

The consistent Sr signature of the soil derived source directly refutes our first hypothesis of an evolving DOC source due to increasing thaw depth as the season progresses. Instead, our $^{87}Sr/^{86}Sr$ data suggests a similar soil-derived source across season likely originating from surface organic horizons.

Critically, our data demonstrates that soil-stream connectivity extends well beyond traditional monitoring, in accordance with our second hypothesis. Associated contributions persist 30+ days past typical late-season cutoffs, well into the first stages of Arctic winter. While this phenomenon is likely to vary in intensity across arctic latitudes, the extended mobilization suggests current Arctic carbon flux models may still underestimate annual DOC export by significantly more than the previously estimated 30% (Kelley et al., 2025a, 2025b; Shogren et al., 2020), particularly if talik-stream connectivity enables continuous winter mobilization (Parazoo et al., 2018; Walter Anthony et al., 2024). This is supported by comparison with larger Arctic rivers, where spring freshet alone accounts for 40–60% of annual DOC export (Chupakov et al., 2020, 2023). However, the gradual autumn decline in soil-stream connectivity that we document suggests that annual DOC export remains underestimated. The lengthening of biogeochemically active seasons observed here aligns with recent findings of extended soil processes under changing Arctic conditions (Villani et al., 2025).

These findings have implications for future Arctic carbon dynamics. As climate warming drives later freeze-up and earlier thaw, these "hidden" shoulder season export windows will expand, potentially mobilizing additional carbon through previously unaccounted pathways. Finally, our results further highlight the critical importance of year-round monitoring in small arctic rivers. While large rivers integrate diverse signals, small catchments like PC provide direct windows into permafrost-carbon dynamics and early warning signals of system change.

CRediT authorship contribution statement

P. Roux: Writing – review & editing, Writing – original draft, Visualization, Methodology, Investigation, Funding acquisition, Formal analysis, Data curation, Conceptualization. **C. Hirst:** Writing – review & editing, Investigation. **M. Villani:** Writing – review & editing, Investigation. **E. du Bois d'Aische:** Writing – review & editing, Investigation. **C. Osy:** Investigation. **A.K. Kelley:** Writing – review & editing, Investigation. **J. Ledman:** Investigation. **E.A.G. Schuur:** Writing – review & editing, Resources, Investigation. **S. Opfergelt:** Writing – review & editing, Supervision, Resources, Investigation, Funding acquisition, Conceptualization.

Declaration of generative AI and AI-assisted technologies in the writing process

This manuscript has been edited with the help of Claude AI and ChatGPT to improve readability, flow, and overall English quality. After using this tool/service, I, the author, reviewed and edited the content as needed. The structure of ideas, argumentative flow and message conveyed by this manuscript remain entirely my own, and I take full responsibility for its content.

Declaration of competing interest

The authors declare that they have no known competing financial interests or personal relationships that could have appeared to influence the work reported in this paper.

Acknowledgment

The authors would like to thank the entire MOCA platform for their help in acquiring the data necessary to produce this manuscript as well as Gilles Denis from Imaqa Expeditions and Maud Henrion for help on the field. This work was supported by BELSPO (RT/23/LIFTHAW).

Appendix A. Supplementary data

Supplementary data to this article can be found online at https://doi.org/10.1016/j.chemgeo.2026.123427.

Data availability

Data will be made available on request.

References

Aciego, S.M., Bourdon, B., Lupker, M., Rickli, J., 2009. A new procedure for separating and measuring radiogenic isotopes (u, th, pa, ra, sr, nd, hf) in ice cores. Chem. Geol. 266 (3–4), 194–204. https://doi.org/10.1016/J.CHEMGEO.2009.06.003.

Aiken, G.R., Spencer, R.G.M., Striegl, R.G., Schuster, P.F., Raymond, P.A., 2014. Influences of glacier melt and permafrost thaw on the age of dissolved organic carbon in the Yukon river basin. Global Biogeochem. Cycles 28 (5), 525–537. https://doi.org/10.1002/2013GB004764.

Alsafi, N.E., Palmer, M.J., Kokelj, S.V., Ensom, T.P., Spence, C., Tank, S.E., 2024. Icings as sentinels and modifiers of water flow through winter landscapes: an exploration of physico-chemical processes on the lake-dominated, discontinuous permafrost taiga shield. Hydrol. Process. 38 (8), e15251. https://doi.org/10.1002/hyp.15251.

Amon, R.M.W., Rinehart, A.J., Duan, S., Louchouarn, P., Prokushkin, A., Guggenberger, G., Bauch, D., Stedmon, C., Raymond, P.A., Holmes, R.M., McClelland, J.W., Peterson, B.J., Walker, S.A., Zhulidov, A.V., 2012. Dissolved organic matter sources in large arctic rivers. Geochim. Cosmochim. Acta 94, 217–237. https://doi.org/10.1016/j.gca.2012.07.015.

Bagard, M.L., Schmitt, A.D., Chabaux, F., Pokrovsky, O.S., Viers, J., Stille, P., Labolle, F., Prokushkin, A.S., 2013. Biogeochemistry of stable ca and radiogenic Sr isotopes in a larch-covered permafrost-dominated watershed of Central Siberia. Geochim. Cosmochim. Acta 114, 169–187. https://doi.org/10.1016/J.GCA.2013.03.038.

Barnes, R.T., Butman, D.E., Wilson, H.F., Raymond, P.A., 2018. Riverine export of aged carbon driven by flow path depth and residence time. Environ. Sci. Tech. 52 (3), 1028–1035. https://doi.org/10.1021/acs.est.7b04717.

Bataille, C.P., Crowley, B.E., Wooller, M.J., Bowen, G.J., 2020. Advances in global bioavailable strontium isoscapes. Palaeogeogr. Palaeoclimatol. Palaeoecol. 555, 109849. https://doi.org/10.1016/J.PALAEO.2020.109849.

Beel, C.R., Heslop, J.K., Orwin, J.F., Pope, M.A., Schevers, A.J., Hung, J.K.Y., Lafrenière, M.J., Lamoureux, S.F., 2021. Emerging dominance of summer rainfall driving high arctic terrestrial-aquatic connectivity. Nat. Commun. 12 (1), 1–9. https://doi.org/10.1038/S41467-021-21759-3.

Birkle, P., Torres-Alvarado, I.S., 2010. Water-rock interaction. In: Water-Rock Interaction, pp. 1–979. https://doi.org/10.1201/9781482242911-16.

Bowen, J.C., Ward, C.P., Kling, G.W., Cory, R.M., 2020. Arctic amplification of global warming strengthened by sunlight oxidation of permafrost carbon to CO2. Geophys. Res. Lett. 47 (12). https://doi.org/10.1029/2020GL087085.

Buckeridge, K.M., Grogan, P., 2010. Deepened snow increases late thaw biogeochemical pulses in Mesic low arctic tundra. Biogeochemistry 101 (1), 105–121.

Burn, C.R., Bartsch, A., Chakraborty, E., Das, S., Frauenfelder, R., Gärtner-Roer, I., Gisnås, K.G., Herring, T., Jones, B.M., Kokelj, S.V., Langer, M., Lathrop, E., Murton, J.B., Nielsen, D.M., Niu, F., Olson, C., O'Neill, H.B., Opfergelt, S., Overduin, P.P., Yarmak, E., 2025. Developments in permafrost science and engineering in response to climate warming in circumpolar and high mountain regions, 2019–2024. Permafr. Periglac. Process. 36 (2), 167–188. https://doi.org/10.1002/PPP.2261.

Capo, R.C., Stewart, B.W., Chadwick, O.A., 1998. Strontium isotopes as tracers of ecosystem processes: theory and methods. Geoderma 82 (1–3), 197–225.

Carey, S.K., Quinton, W.L., 2005. Evaluating runoff generation during summer using hydrometric, stable isotope and hydrochemical methods in a discontinuous permafrost alpine catchment. Hydrol. Process. 19 (1), 95–114. https://doi.org/10.1002/hyp.5764.

Carey, S.K., Woo, M., 2002. Hydrogeomorphic relations among soil pipes, flow pathways, and soil detachments within a permafrost hillslope. Phys. Geogr. 23 (2), 95–114. https://doi.org/10.2747/0272-3646.23.2.95.

Catalán, N., Pastor, A., Borrego, C.M., Casas-Ruiz, J.P., Hawkes, J.A., Gutiérrez, C., von Schiller, D., Marcé, R., 2021. The relevance of environment vs. composition on dissolved organic matter degradation in freshwaters. Limnol. Oceanogr. 66 (2), 306–320. https://doi.org/10.1002/LNO.11606.

Chadwick, O.A., Derry, L.A., Vitousek, P.M., Huebert, B.J., Hedin, L.O., 1999. Changing sources of nutrients during four million years of ecosystem development. Nature 397 (6719), 491–497. https://doi.org/10.1038/17276.

Chupakov, A.V., Pokrovsky, O.S., Moreva, O.Y., Shirokova, L.S., Neverova, N.V., Chupakova, A.A., Kotova, E.I., Vorobyeva, T.Y., 2020. High resolution multi-annual riverine fluxes of organic carbon, nutrient and trace element from the largest european arctic river, Severnaya Dvina. Chem. Geol. 538, 119491. https://doi.org/10.1016/j.chemgeo.2020.119491.

Chupakov, A.V., Pokrovsky, O.S., Moreva, O.Y., Kotova, E.I., Vorobyeva, T.Y., Shirokova, L.S., 2023. Export of organic carbon, nutrients and metals by the mid-sized Pechora river to the arctic ocean. Chem. Geol. 632, 121524. https://doi.org/10.1016/j.chemgeo.2023.121524.

Clark, I.D., Fritz, P., 1997. Environmental isotopes in hydrogeology. In: Chapter, 9. Water–Rock Interaction. CRC Press/Lewis Publishers, Boca Raton, FL. https://doi.org/10.1201/9781482242911.

Clayton, R.N., O'Neil, J.R., Mayeda, T.K., 1972. Oxygen isotope exchange between quartz and water. J. Geophys. Res. 77 (17), 3057–3067. https://doi.org/10.1029/JB077I017P03057.

Cory, R.M., Ward, C.P., Crump, B.C., Kling, G.W., 2014. Sunlight controls water column processing of carbon in arctic fresh waters. Science 345 (6199), 925–928. https://doi.org/10.1126/SCIENCE.1253119.

Dean, J.F., Meisel, O.H., Martyn Rosco, M., Marchesini, L.B., Garnett, M.H., Lenderink, H., van Logtestijn, R., Borges, A.V., Bouillon, S., Lambert, T., Röckmann, T., Maximov, T., Petrov, R., Karsanaev, S., Aerts, R., van Huissteden, J., Vonk, J.E., Dolman, A.J., 2020. East Siberian arctic inland waters emit mostly contemporary carbon. Nat. Commun. 11 (1), 1–10. https://doi.org/10.1038/S41467-020-15511-6.

Devoie, E., Connon, R.F., Beddoe, R., Goordial, J., Quinton, W.L., Craig, J.R., 2024. Disconnected active layers and unfrozen permafrost: a discussion of permafrost-related terms and definitions. Sci. Total Environ. 912, 169017. https://doi.org/10.1016/J.SCITOTENV.2023.169017.

Douglas, T.A., Torre Jorgenson, M., Brown, D.R.N., Campbell, S.W., Hiemstra, C.A., Saari, S.P., Bjella, K., Liljedahl, A.K., 2016. Degrading permafrost mapped with electrical resistivity tomography, airborne imagery and LiDAR, and seasonal thaw measurements. Geophysics 81 (1), WA71–WA85. https://doi.org/10.1190/GEO2015-0149.1.

Farquharson, L.M., Romanovsky, V.E., Kholodov, A., Nicolsky, D., 2022. Sub-aerial talik formation observed across the discontinuous permafrost zone of Alaska. Nat. Geosci. 15 (6), 475–481. https://doi.org/10.1038/S41561-022-00952-Z.

Finlay, J., Neff, J., Zimov, S., Davydova, A., Davydov, S., 2006. Snowmelt dominance of dissolved organic carbon in high-latitute watersheds: implications for characterization and flux of river DOC. Geophys. Res. Lett. 33 (10). https://doi.org/10.1029/2006GL025754.

Frey, K.E., McClelland, J.W., 2009. Impacts of permafrost degradation on arctic river biogeochemistry. Hydrol. Process. 23 (1), 169–182. https://doi.org/10.1002/HYP.7196.

Frey, K.E., Siegel, D.I., Smith, L.C., 2007. Geochemistry of west siberian streams and their potential response to permafrost degradation. Water Resour. Res. 43 (3), 3406. https://doi.org/10.1029/2006WR004902.

Gagné, K.R., Ewers, S.C., Murphy, C.J., Daanen, R., Walter Anthony, K., Guerard, J.J., 2020. Composition and photo-reactivity of organic matter from permafrost soils and surface waters in interior Alaska. Environ. Sci.: Processes Impacts 22 (7), 1525–1539. https://doi.org/10.1039/d0em00097c.

Gibson, J.J., Prowse, T.D., 2002. Stable isotopes in river ice: Identifying primary over-winter streamflow signals and their hydrological significance. Hydrol. Process. 16 (4), 873–890. https://doi.org/10.1002/HYP.366.

Guo, L., Cai, Y., Belzile, C., Macdonald, R.W., 2012. Sources and export fluxes of inorganic and organic carbon and nutrient species from the seasonally ice-covered Yukon river. Biogeochemistry 107 (1–3), 187–206. https://doi.org/10.1007/S10533-010-9545-Z.

Heaton, T.J., Bard, E., Ramsey, C.B., Butzin, M., Köhler, P., Muscheler, R., Reimer, P.J., Wacker, L., 2021. Radiocarbon: a key tracer for studying earths dynamo, climate system, carbon cycle, and sun. Science 374 (6568). https://doi.org/10.1126/SCIENCE.ABD7096.

Hirst, C., Mauclet, E., Monhonval, A., Tihon, E., Ledman, J., Schuur, E.A.G., Opfergelt, S., 2022. Seasonal changes in hydrology and permafrost degradation control mineral Element-Bound DOC transport from permafrost soils to streams. Global Biogeochem. Cycles 36 (2). https://doi.org/10.1029/2021GB007105.

Humborg, C., Mörth, C.M., Sundbom, M., Borg, H., Blenckner, T., Giesler, R., Ittekkot, V., 2010. CO2 supersaturation along the aquatic conduit in Swedish watersheds as constrained by terrestrial respiration, aquatic respiration and weathering. Glob. Chang. Biol. 16 (7), 1966–1978. https://doi.org/10.1111/J.1365-2486.2009.02092.X.

Hutchings, J.A., Bianchi, T.S., Kaufman, D.S., Kholodov, A.L., Vaughn, D.R., Schuur, E.A.G., 2019. Millennial-scale carbon accumulation and molecular transformation in a permafrost core from interior Alaska. Geochim. Cosmochim. Acta 253, 231–248. https://doi.org/10.1016/j.gca.2019.03.028.

Ilina, S.M., Lapitskiy, S.A., Alekhin, Y.V., Viers, J., Benedetti, M., Pokrovsky, O.S., 2015. Speciation, size fractionation and transport of trace elements in the continuum soil Water–Mire–Humic Lake–River–large oligotrophic lake of a subarctic watershed. Aquat. Geochem. 22 (1), 65–95. https://doi.org/10.1007/S10498-015-9277-8.

Jafarov, E.E., Coon, E.T., Harp, D.R., Wilson, C.J., Painter, S.L., Atchley, A.L., Romanovsky, V.E., 2018. Modeling the role of preferential snow accumulation in through talik development and hillslope groundwater flow in a transitional permafrost landscape. Environ. Res. Lett. 13 (10), 105006. https://doi.org/10.1088/1748-9326/AADD30.

Jones, M.C., Grosse, G., Treat, C., Turetsky, M., Anthony, K.W., Brosius, L., 2023. Past permafrost dynamics can inform future permafrost carbon-climate feedbacks. Commun. Earth Environ. 4 (1), 1–13. https://doi.org/10.1038/s43247-023-00886-3.

Juhls, B., Stedmon, C.A., Morgenstern, A., Meyer, H., Hölemann, J., Heim, B., Povazhnyi, V., Overduin, P.P., 2020. Identifying drivers of seasonality in Lena river biogeochemistry and dissolved organic matter fluxes. Front. Environ. Sci. 8, 529726. https://doi.org/10.3389/FENVS.2020.00053.

Karolytė, R., Serno, S., Johnson, G., Gilfillan, S.M.V., 2017. The influence of oxygen isotope exchange between CO2 and H2O in natural CO2-rich spring waters: implications for geothermometry. Appl. Geochem. 84, 173–186. https://doi.org/10.1016/J.APGEOCHEM.2017.06.012.

Keller, K., Blum, J.D., Kling, G.W., 2010. Stream geochemistry as an indicator of increasing permafrost thaw depth in an arctic watershed. Chem. Geol. 273 (1–2), 76–81. https://doi.org/10.1016/j.chemgeo.2010.02.013.

Kelley, A.K., Axler, Z., Ledman, J., De La Torre, M., Ebert, C.H., Springer, A.E., Kaufman, D.S., Schuur, E.A.G., 2025a. Lateral dissolved organic carbon losses represent ~10% of upland tundra carbon losses and include seasonal permafrost contributions. J. Geophys. Res. Biogeosci. 130 (11), e2025JG009067. https://doi.org/10.1029/2025JG009067.

Kelley, A.K., Pegoraro, E., Mauritz, M., Hutchings, J., Natali, S., Hicks-Pries, C.E., Schuur, E., LTER, B. C., 2025b. Eight Mile Lake Research Watershed, Thaw Gradient: Seasonal Thaw Depth 2004–2024. https://doi.org/10.6073/PASTA/54FEB1D2D53564E3C16FAA64D2A6AA02.

Kennedy, Elliot, Celis, Gerardo, See, Craig R., Schaedel, Christina, Mauritz, Marguerite, Taylor, Meghan, Ledman, Justin, Natali, Susan, Schuur, Edward, 2025. Eight Mile Lake Research Watershed: Hourly Meteorological Data, 2004-2025. Bonanza Creek LTER - University of Alaska Fairbanks. BNZ:453. http://www.lter.uaf.edu/data/data-detail/id/453. https://doi.org/10.6073/pasta/c1b76570a7f3d4feaef428e98970b2be.

Koch, J.C., O'Donnell, J.A., 2025. Observing northern high-latitude river systems to understand changes in a warming Arctic. Curr. Clim. Change Rep. 11 (1), 5. https://doi.org/10.1007/S40641-025-00202-5.

Koch, J.C., Runkel, R.L., Striegl, R., McKnight, D.M., 2013. Hydrologic controls on the transport and cycling of carbon and nitrogen in a boreal catchment underlain by continuous permafrost. J. Geophys. Res. Biogeo. 118 (2), 698–712. https://doi.org/10.1002/JGRG.20058.

Koch, J.C., Bogard, M.J., Butman, D.E., Finlay, K., Ebel, B., James, J., Johnston, S.E., Jorgenson, M.T., Pastick, N.J., Spencer, R.G.M., Striegl, R., Walvoord, M., Wickland, K.P., 2022. Heterogeneous patterns of aged organic carbon export driven by hydrologic flow paths, soil texture, fire, and thaw in discontinuous permafrost headwaters. Global Biogeochem. Cycles 36 (4). https://doi.org/10.1029/2021GB007242.

Kokelj, S.V., Tunnicliffe, J., Lacelle, D., Lantz, T.C., Chin, K.S., Fraser, R., 2015. Increased precipitation drives mega slump development and destabilization of ice-rich permafrost terrain, northwestern Canada. Global Planet. Change 129, 56–68. https://doi.org/10.1016/J.GLOPLACHA.2015.02.008.

Krickov, I.V., Pokrovsky, O.S., Manasypov, R.M., Lim, A.G., Shirokova, L.S., Viers, J., 2019. Colloidal transport of carbon and metals by western Siberian rivers during different seasons across a permafrost gradient. Geochim. Cosmochim. Acta 265, 221–241. https://doi.org/10.1016/j.gca.2019.08.041.

Krickov, I.V., Loiko, S.V., Lim, A.G., Kuzmina, D.M., Istigechev, G.I., Shirokova, L.S., Pupyshev, Y.S., Pokrovsky, O.S., 2026. Hydrological continuums across climate and permafrost gradients: Spatial patterns of organic carbon, greenhouse gases, and major and trace elements. Water Res. 294 (3), 125507. https://doi.org/10.1016/j.watres.2026.125507.

Lang, S.Q., McIntyre, C.P., Bernasconi, S.M., Früh-Green, G.L., Voss, B.M., Eglinton, T.I., Wacker, L., 2016. Rapid 14C analysis of dissolved organic carbon in non-saline waters. Radiocarbon 58 (3), 505–515. https://doi.org/10.1017/RDC.2016.17.

Lathrop, E., See, C., Walker, X., Falvo, G., Axler, Z., Ebert, C., Kadej, S., Kelley, A., Ledman, J., Opfergelt, S., Rodenhizer, H., Schuur, E.A.G., 2025. Permafrost thaw accelerates old soil carbon release, outpacing new plant inputs during a 13-year tundra warming experiment. Glob. Chang. Biol. 31 (12), e70609. https://doi.org/10.1111/gcb.70609.

Laudon, H., Seibert, J., Köhler, S., Bishop, K., 2004. Hydrological flow paths during snowmelt: congruence between hydrometric measurements and oxygen 18 in meltwater, soil water, and runoff. Water Resour. Res. 40 (3), 3102. https://doi.org/10.1029/2003WR002455.

Liu, S., Wang, P., Huang, Q., Yu, J., Pozdniakov, S.P., Kazak, E.S., 2022. Seasonal and spatial variations in riverine DOC exports in permafrost-dominated arctic river basins. J. Hydrol. 612, 128060. https://doi.org/10.1016/j.jhydrol.2022.128060.

Mann, P.J., Eglinton, T.I., McIntyre, C.P., Zimov, N., Davydova, A., Vonk, J.E., Holmes, R.M., Spencer, R.G.M., 2015. Utilization of ancient permafrost carbon in headwaters of arctic fluvial networks. Nat. Commun. 6 (1), 1–7. https://doi.org/10.1038/NCOMMS8856.

Marshall, L.P., Kaufman, D.S., Anderson, R.S., McKay, N.P., Schuur, E.A.G., 2023. Organic-Matter accumulation and degradation in Holocene permafrost deposits along a Central Alaska hillslope. J. Geophys. Res. 128 (9), e2022JG007290. https://doi.org/10.1029/2022JG007290.

Matsuhisa, Y., Goldsmith, J.R., Clayton, R.N., 1979. Oxygen isotopic fractionation in the system quartz-albite-anorthite-water. Geochim. Cosmochim. Acta 43 (7), 1131–1140. https://doi.org/10.1016/0016-7037(79)90099-1.

Mauclet, E., Hirst, C., Monhonval, A., Stevenson, E.I., Gérard, M., Villani, M., Dailly, H., Schuur, E.A.G., Opfergelt, S., 2023. Tracing changes in base cation sources for Arctic Tundra vegetation upon permafrost thaw. Geoderma 429, 116277. https://doi.org/10.1016/J.GEODERMA.2022.116277.

McKenzie, J.M., Voss, C.I., 2013. Permafrost thaw in a nested groundwater-flow system. Hydrogeol. J. 21 (1), 299–316. https://doi.org/10.1007/s10040-012-0942-3.

Meredith, M., Sommerkorn, M., Cassotta, S., Derksen, C., Ekaykin, A., Hollowed, A., Kofinas, G., Mackintosh, A., Melbourne-Thomas, J., Muelbert, M.M.C., 2019. Polar Regions. Chapter 3, IPCC Special Report on the Ocean and Cryosphere in a Changing Climate.

Monhonval, A., Hirst, C., Strauss, J., Schuur, E.A.G., Opfergelt, S., 2023. Strontium isotopes trace the dissolution and precipitation of mineral organic carbon interactions in thawing permafrost. Geoderma 433, 116456. https://doi.org/10.1016/J.GEODERMA.2023.116456.

Mu, C., Li, K., Liu, S., Wei, Y., Mu, M., Shang, X., Liu, F., Zhang, C., Liu, H., Gao, T., Song, C., Zhang, L., Karlsson, J., 2025. Recent intensified riverine CO2 emission across the northern hemisphere permafrost region. Nat. Commun. 16 (1), 1–11. https://doi.org/10.1038/S41467-025-58716-3.

Neff, J.C., Finlay, J.C., Zimov, S.A., Davydov, S.P., Carrasco, J.J., Schuur, E.A.G., Davydova, A.I., 2006. Seasonal changes in the age and structure of dissolved organic carbon in Siberian rivers and streams. Geophys. Res. Lett. 33 (23). https://doi.org/10.1029/2006GL028222.

Obu, J., 2021. How much of the earths surface is underlain by permafrost? J. Geophys. Res.: Earth Surf. 126 (5), e2021JF006123. https://doi.org/10.1029/2021JF006123.

O'Donnell, J.A., Aiken, G.R., Walvoord, M.A., Butler, K.D., 2012. Dissolved organic matter composition of winter flow in the Yukon river basin: Implications of permafrost thaw and increased groundwater discharge. Global Biogeochem. Cycles 26 (4). https://doi.org/10.1029/2012GB004341.

O'Donnell, J.A., Aiken, G.R., Walvoord, M.A., Raymond, P.A., Butler, K.D., Dornblaser, M.M., Heckman, K., 2014. Using dissolved organicmatter age and composition to detect permafrost thaw in boreal watersheds of interior Alaska.

J. Geophys. Res. Biogeo. 119 (11), 2155–2170. https://doi.org/10.1002/2014JG002695.
Olsson, P.Q., Sturm, M., Racine, C.H., Romanovsky, V., Liston, G.E., 2003. Five stages of the Alaskan Arctic cold season with ecosystem implications. Arct. Antarct. Alp. Res. 35 (1), 74–81. https://www.jstor.org/stable/1552331.
Opfergelt, S., Gaspard, F., Hirst, C., Monin, L., Juhls, B., Morgenstern, A., Angelopoulos, M., Overduin, P.P., 2024. Frazil ice changes winter biogeochemical processes in the Lena river. Commun. Earth Environ. 5 (1), 1–8. https://doi.org/10.1038/s43247-024-01884-9.
Osterkamp, T.E., Jorgenson, M.T., Schuur, E.A.G., Shur, Y.L., Kanevskiy, M.Z., Vogel, J. G., Tumskoy, V.E., 2009. Physical and ecological changes associated with warming permafrost and thermokarst in interior Alaska. Permafr. Periglac. Process. 20 (3), 235–256. https://doi.org/10.1002/PPP.656.
Parazoo, N.C., Koven, C.D., Lawrence, D.M., Romanovsky, V., Miller, C.E., 2018. Detecting the permafrost carbon feedback: Talik formation and increased cold-season respiration as precursors to sink-to-source transitions. Cryosphere 12 (1), 123–144. https://doi.org/10.5194/TC-12-123-2018.
Peng, X., Zhang, T., Frauenfeld, O.W., Mu, C., Wang, K., Wu, X., Guo, D., Luo, J., Hjort, J., Aalto, J., Karjalainen, O., Luoto, M., 2023. Active layer thickness and permafrost area projections for the 21st century. Earth's Future 11 (8), e2023EF003573. https://doi.org/10.1029/2023EF003573.
Petrone, K.C., Jones, J.B., Hinzman, L.D., Boone, R.D., 2006. Seasonal export of carbon, nitrogen, and major solutes from Alaskan catchments with discontinuous permafrost. J. Geophys. Res. Biogeo. 111 (2), 2020. https://doi.org/10.1029/2005JG000055.
Plaza, C., Pegoraro, E., Bracho, R., Celis, G., Crummer, K.G., Hutchings, J.A., Hicks Pries, C.E., Mauritz, M., Natali, S.M., Salmon, V.G., Schädel, C., Webb, E.E., Schuur, E.A.G., 2019. Direct observation of permafrost degradation and rapid soil carbon loss in tundra. Nat. Geosci. 12 (8), 627–631. https://doi.org/10.1038/S41561-019-0387-6;SUBJMETA=106,158,47,704.
Pokrovsky, O.S., Schott, J., 2002. Iron colloids/organic matter associated transport of major and trace elements in small boreal rivers and their estuaries (NW Russia). Chem. Geol. 190 (1–4), 141–179. https://doi.org/10.1016/S0009-2541(02)00115-8.
Pokrovsky, O.S., Manasypov, R.M., Loiko, S., Shirokova, L.S., Krickov, I.A., Pokrovsky, B. G., Kolesnichenko, L.G., Kopysov, S.G., Zemtzov, V.A., Kulizhsky, S.P., Vorobyev, S. N., Kirpotin, S.N., 2015. Permafrost coverage, watershed area and season control of dissolved carbon and major elements in western siberian rivers. Biogeosciences 12 (21), 6301–6320. https://doi.org/10.5194/bg-12-6301-2015.
Putman, A.L., Fiorella, R.P., Bowen, G.J., Cai, Z., 2019. A global perspective on local meteoric water lines: meta-analytic insight into fundamental controls and practical constraints. Water Resour. Res. 55 (8), 6896–6910. https://doi.org/10.1029/2019WR025181.
Raymond, P.A., McClelland, J.W., Holmes, R.M., Zhulidov, A.V., Mull, K., Peterson, B.J., Striegl, R.G., Aiken, G.R., Gurtovaya, T.Y., 2007. Flux and age of dissolved organic carbon exported to the Arctic ocean: a carbon isotopic study of the five largest Arctic rivers. Global Biogeochem. Cycles 21 (4). https://doi.org/10.1029/2007GB002934.
Reynolds, A.C., Quade, J., Betancourt, J.L., 2012. Strontium isotopes and nutrient sourcing in a semi-arid woodland. Geoderma 189–190, 574–584. https://doi.org/10.1016/J.GEODERMA.2012.06.029.
Rocher-Ros, G., Harms, T.K., Sponseller, R.A., Väisänen, M., Mörth, C.M., Giesler, R., 2021. Metabolism overrides photo-oxidation in CO2 dynamics of Arctic permafrost streams. Limnol. Oceanogr. 66 (S1), S169–S181. https://doi.org/10.1002/LNO.11564.
Rodenhizer, H., Ledman, J., Mauritz, M., Natali, S.M., Pegoraro, E., Plaza, C., Romano, E., Schädel, C., Taylor, M., Schuur, E., 2020. Carbon thaw rate doubles when accounting for subsidence in a permafrost warming experiment. J. Geophys. Res. 125 (6), e2019JG005528. https://doi.org/10.1029/2019JG005528.
Rushlow, C.R., Godsey, S.E., 2017. Rainfall–runoff responses on arctic hillslopes underlain by continuous permafrost, North Slope, Alaska, USA. Hydrol. Process. 31 (23), 4092–4106. https://doi.org/10.1002/HYP.11294.
Schaefer, K., Lantuit, H., Romanovsky, V.E., Schuur, E.A.G., Witt, R., 2014. The impact of the permafrost carbon feedback on global climate. Environ. Res. Lett. 9 (8), 85003.
Schuur, E.A.G., Bockheim, J., Canadell, J.G., Euskirchen, E., Field, C.B., Goryachkin, S. V., Hagemann, S., Kuhry, P., Lafleur, P.M., Lee, H., Mazhitova, G., Nelson, F.E., Rinke, A., Romanovsky, V.E., Shiklomanov, N., Tarnocai, C., Venevsky, S., Vogel, J. G., Zimov, S.A., 2008. Vulnerability of permafrost carbon to climate change: implications for the global carbon cycle. BioScience 58 (8), 701–714. https://doi.org/10.1641/B580807.
Schuur, E.A.G., Vogel, J.G., Crummer, K.G., Lee, H., Sickman, J.O., Osterkamp, T.E., 2009. The effect of permafrost thaw on old carbon release and net carbon exchange from tundra. Nature 459 (7246), 556–559. https://doi.org/10.1038/NATURE08031.
Schuur, E.A.G., McGuire, A.D., Schädel, C., Grosse, G., Harden, J.W., Hayes, D.J., Hugelius, G., Koven, C.D., Kuhry, P., Lawrence, D.M., Natali, S.M., Olefeldt, D., Romanovsky, V.E., Schaefer, K., Turetsky, M.R., Treat, C.C., Vonk, J.E., 2015. Climate change and the permafrost carbon feedback. Nature 520 (7546), 171–179. https://doi.org/10.1038/NATURE14338.
Schuur, E.A.G., Abbott, B.W., Commane, R., Ernakovich, J., Euskirchen, E., Hugelius, G., Grosse, G., Jones, M., Koven, C., Leshyk, V., Lawrence, D., Loranty, M.M., Mauritz, M., Olefeldt, D., Natali, S., Rodenhizer, H., Salmon, V., Schädel, C., Strauss, J., Turetsky, M., 2022. Permafrost and climate change: carbon cycle feedbacks from the warming Arctic. Ann. Rev. Environ. Resour. 47 (2022), 343–371. https://doi.org/10.1146/ANNUREV-ENVIRON-012220-011847/1.
Schuur, E.A.G., Hicks Pries, C., Mauritz, M., Pegoraro, E., Rodenhizer, H., See, C., Ebert, C., 2023. Ecosystem and Soil Respiration Radiocarbon Detects Old Carbon Release as a Fingerprint of Warming and Permafrost Destabilization With Climate Change. Royalsocietypublishing.OrgEAG Schuur, C Hicks Pries, M Mauritz, E Pegoraro, H Rodenhizer, C See, C EbertPhilosophical Transactions of the Royal Society A, 2023•royalsocietypublishing.Org, 381(2261). https://doi.org/10.1098/rsta.2022.0201.
Schwab, M.S., Hilton, R.G., Raymond, P.A., Haghipour, N., Amos, E., Tank, S.E., Holmes, R.M., Tipper, E.T., Eglinton, T.I., 2020. An abrupt aging of dissolved organic carbon in large Arctic rivers. Geophys. Res. Lett. 47 (23). https://doi.org/10.1029/2020GL088823.
Serreze, M.C., Barry, R.G., 2011. Processes and impacts of arctic amplification: a research synthesis. Global Planet. Change 77 (1–2), 85–96. https://doi.org/10.1016/J.GLOPLACHA.2011.03.004.
Shogren, A.J., Zarnetske, J.P., Abbott, B.W., Iannucci, F., Frei, R.J., Griffin, N.A., Bowden, W.B., 2019. Revealing biogeochemical signatures of arctic landscapes with river chemistry. Sci. Rep. 9 (1), 1–11. https://doi.org/10.1038/S41598-019-49296-6.
Shogren, A.J., Zarnetske, J.P., Abbott, B.W., Iannucci, F., Bowden, W.B., 2020. We cannot shrug off the shoulder seasons: addressing knowledge and data gaps in an arctic headwater. Environ. Res. Lett. 15 (10), 104027. https://doi.org/10.1088/1748-9326/AB9D3C.
Spencer, R.G.M., Mann, P.J., Dittmar, T., Eglinton, T.I., McIntyre, C., Holmes, R.M., Zimov, N., Stubbins, A., 2015. Detecting the signature of permafrost thaw in arctic rivers. Geophys. Res. Lett. 42 (8), 2830–2835. https://doi.org/10.1002/2015GL063498.
Stolpe, B., Guo, L., Shiller, A.M., Aiken, G.R., 2013. Abundance, size distributions and trace-element binding of organic and iron-rich nanocolloids in Alaskan rivers, as revealed by field-flow fractionation and ICP-MS. Geochim. Cosmochim. Acta 105, 221–239. https://doi.org/10.1016/J.GCA.2012.11.018.
Strauss, J., Fuchs, M., Hugelius, G., Miesner, F., Nitze, I., Opfergelt, S., Schuur, E., Treat, C., Turetsky, M., Yang, Y., Grosse, G., 2025. Organic matter storage and vulnerability in the permafrost domain. In: Encyclopedia of Quaternary Science, pp. 399–410. https://doi.org/10.1016/B978-0-323-99931-1.00164-1.
Streletskiy, D.A., Tananaev, N.I., Opel, T., Shiklomanov, N.I., Nyland, K.E., Streletskaya, I.D., Shiklomanov, A.I., 2015. Permafrost hydrology in changing climatic conditions: seasonal variability of stable isotope composition in rivers in discontinuous permafrost. Environ. Res. Lett. 10 (9), 95003.
Tank, S.E., Vonk, J.E., Walvoord, M.A., McClelland, J.W., Laurion, I., Abbott, B.W., 2020. Landscape matters: predicting the biogeochemical effects of permafrost thaw on aquatic networks with a state factor approach. Permafr. Periglac. Process. 31 (3), 358–370. https://doi.org/10.1002/PPP.2057.
Tank, S.E., McClelland, J.W., Spencer, R.G.M., Shiklomanov, A.I., Suslova, A., Moatar, F., Amon, R.M.W., Cooper, L.W., Elias, G., Gordeev, V.V., Guay, C., Gurtovaya, T.Y., Kosmenko, L.S., Mutter, E.A., Peterson, B.J., Peucker-Ehrenbrink, B., Raymond, P.A., Schuster, P.F., Scott, L., Holmes, R.M., 2023. Recent trends in the chemistry of major northern rivers signal widespread Arctic change. Nat. Geosci. 16 (9), 789–796. https://doi.org/10.1038/s41561-023-01247-7.
Townsend-Small, A., McClelland, J.W., Holmes, R.M., Peterson, B.J., 2011. Seasonal and hydrologic drivers of dissolved organic matter and nutrients in the Upper Kuparuk River, Alaskan Arctic. Biogeochemistry 103 (1), 109–124. https://doi.org/10.1007/S10533-010-9451-4/TABLES/2.
Treat, C.C., Wollheim, W.M., Varner, R.K., Bowden, W.B., 2016. Longer thaw seasons increase nitrogen availability for leaching during fall in tundra soils. Environ. Res. Lett. 11 (6), 064013. https://doi.org/10.1088/1748-9326/11/6/064013.
Trumbore, S., 2000. Age of soil organic matter and soil respiration: radiocarbon constraints on belowground C dynamics. Ecol. Appl. 10 (2), 399–411. https://doi.org/10.1890/1051-0761(2000)010[0399:AOSOMA]2.0.CO;2.
Turetsky, M.R., Abbott, B.W., Jones, M.C., Anthony, K.W., Olefeldt, D., Schuur, E.A.G., Grosse, G., Kuhry, P., Hugelius, G., Koven, C., Lawrence, D.M., Gibson, C., Sannel, A. B.K., McGuire, A.D., 2020. Carbon release through abrupt permafrost thaw. Nat. Geosci. 13 (2), 138–143. https://doi.org/10.1038/S41561-019-0526-0.
Villani, M., Hirst, C., du Boisd' Aische, E., Thomas, M., Lundin, E., Giesler, R., Mörth, C.-M., Opfergelt, S., 2025. Lengthening of biogeochemical processes during winter in degraded permafrost soils. Geochem. Perspect. Lett. 34, 36–42. https://doi.org/10.7185/geochemlet.2511.
Vonk, J.E., Tank, S.E., Walvoord, M.A., 2019. Integrating hydrology and biogeochemistry across frozen landscapes. Nat. Commun. 10 (1), 1–4. https://doi.org/10.1038/S41467-019-13361-5;SUBJMETA=242,47,704.
Vonk, J.E., Speetjens, N.J., Poste, A.E., 2023. Small watersheds may play a disproportionate role in arctic land-ocean fluxes. Nat. Commun. 14 (1), 1–3. https://doi.org/10.1038/S41467-023-39209-7.
U.S. Geological Survey. National hydrography dataset ver. (version USGS national hydrography dataset best resolution (NHD) for Hydrologic Unit (HU) 12 [Dataset]. https://www.usgs.gov/national-hydrography/access-national-hydrography-products. Retrieved from.
Vonk, J.E., Fritz, M., Speetjens, N.J., Babin, M., Bartsch, A., Basso, L.S., Bröder, L., Göckede, M., Gustafsson, Ö., Hugelius, G., Irrgang, A.M., Juhls, B., Kuhn, M.A., Lantuit, H., Manizza, M., Martens, J., O'Regan, M., Suslova, A., Tank, S.E., Zolkos, S., 2025. The land–ocean arctic carbon cycle. Nat. Rev. Earth Environ. 6 (2), 86–105. https://doi.org/10.1038/S43017-024-00627-W.
Walter Anthony, K.M., Anthony, P., Hasson, N., Edgar, C., Sivan, O., Eliani-Russak, E., Bergman, O., Minsley, B.J., James, S.R., Pastick, N.J., Kholodov, A., Zimov, S., Euskirchen, E., Bret-Harte, M.S., Grosse, G., Langer, M., Nitzbon, J., 2024. Upland Yedoma taliks are an unpredicted source of atmospheric methane. Nat. Commun. 15 (1), 6056. https://doi.org/10.1038/s41467-024-50346-5.
Walvoord, M.A., Striegl, R.G., 2021. Complex vulnerabilities of the water and aquatic carbon cycles to permafrost thaw. Front. Clim. 3, 730402. https://doi.org/10.3389/fclim.2021.730402.

Walvoord, M.A., Voss, C.I., Ebel, B.A., Minsley, B.J., 2019. Development of perennial thaw zones in boreal hillslopes enhances potential mobilization of permafrost carbon. Environ. Res. Lett. 14 (1), 015003. https://doi.org/10.1088/1748-9326/aaf0cc.

Wild, B., Andersson, A., Bröder, L., Vonk, J., Hugelius, G., McClelland, J.W., Song, W., Raymond, P.A., Gustafsson, Ö., 2019. Rivers across the Siberian Arctic unearth the patterns of carbon release from thawing permafrost. Proc. Natl. Acad. Sci. U. S. A. 116 (21), 10280–10285. https://doi.org/10.1073/pnas.1811797116.

Wortberg, K., Conrad, S., Andersson, P.S., Ingri, J., 2017. Strontium isotopes – a tracer for river suspended iron aggregates. Appl. Geochem. 79, 85–90. https://doi.org/10.1016/J.APGEOCHEM.2017.02.012.

Yi, Y., Gibson, J.J., Hélie, J.F., Dick, T.A., 2010. Synoptic and time-series stable isotope surveys of the Mackenzie River from Great Slave Lake to the Arctic Ocean, 2003 to 2006. J. Hydrol. 383 (3–4), 223–232. https://doi.org/10.1016/J.JHYDROL.2009.12.038.

Zhang, Z., Liu, F., Chen, S., Zhang, J., Jiang, W., Ning, H., Liu, W., Gao, Z., Cao, W., Guo, H., 2025. Strontium isotope and multi-tracer insights into groundwater mixing and fluoride mobilization in the Luanhe River Delta, Northern China. Appl. Geochem. 193, 106567. https://doi.org/10.1016/J.APGEOCHEM.2025.106567.